Research Square

Preprints are preliminary reports that have not undergone peer review.
They should not be considered conclusive, used to inform clinical practice,
or referenced by the media as validated information.

# Leveraging Quantum Uncertainty for Modeling Financial Volatility via Quantum Reservoir Computing

**Aryan Polakhare**
LIRA Centre, Lancaster University
**Wenyi Ge**
LIRA Centre, Lancaster University
**Richard Jiang**
r.jiang2@lancaster.ac.uk

LIRA Centre, Lancaster University

**Research Article**

**Keywords:** Quantum Reservoir Computing, Quantum Machine Learning, Quantum Uncertainty, Financial Forecasting, Entanglement, Temporal Modeling, Stochastic Systems, Quantum Advantage

**Posted Date:** November 2nd, 2026

**DOI:** https://doi.org/10.21203/rs.3.rs-8063872/v1

**License:** This work is licensed under a Creative Commons Attribution 4.0 International License.
Read Full License

**Additional Declarations:** Competing interest reported. \section*{Acknowledgements} The authors thank the LIRA Centre at Lancaster University for providing computational resources and research infrastructure. They gratefully acknowledge valuable discussions with colleagues in quantum computing and financial modelling that helped shape this research, and they thank the wider quantum computing community for developing the open-source tools (PennyLane, Qiskit, and Cirq) that made this work possible. The authors also thank the anonymous reviewers for their constructive feedback, which substantially improved the manuscript, and acknowledge the broader quantum machine-learning community for establishing the theoretical foundations that enabled this study. \section*{Funding Declaration} This research was supported by the UK Engineering and Physical Sciences Research Council (EPSRC) under Grant EP/P009727/2 and by the Leverhulme Trust under Grant RF–2019–492. Additional computational resources were provided by the UK National High-Performance Computing facility through allocated time grants. \section*{Competing interests} The authors declare no competing

financial interests related to this work. Neither author has financial relationships with quantum computing companies, financial trading firms, or investment management organizations that could bias the research outcomes. No patents have been filed related to the methods described in this work. The research was conducted purely for academic purposes without commercial considerations. All software tools used were open-source or freely available academic licenses. No proprietary quantum computing platforms or commercial financial data services were used in ways that would create conflicts of interest.

# Leveraging Quantum Uncertainty for Modeling Financial Volatility via Quantum Reservoir Computing

Aryan Polakhare[1,2], Wenyi Ge[1,2], Richard Jiang[1,2*]

[1*]LIRA Centre, Lancaster University, Lancaster, LA1 4YW, United Kingdom.

[2]Quantum Technology Centre, Lancaster University, Lancaster, LA1 4YB, United Kingdom.

*Corresponding author(s). E-mail(s): r.jiang2@lancaster.ac.uk;
Contributing authors: a.polakhare@lancaster.ac.uk;
w.ge4@lancaster.ac.uk;

**Abstract**

Financial markets exhibit complex non-linear dynamics, temporal dependencies, and stochastic volatility, posing enduring challenges for classical forecasting models. Quantum computing provides a fundamentally different computational paradigm, exploiting superposition, entanglement, and quantum interference to encode and process information in richer representational spaces. Here, we introduce the Entangled Quantum Coherent Reservoir Network (eQCRN) — a quantum reservoir computing framework that leverages quantum uncertainty to model financial uncertainty. eQCRN integrates multiple quantum reservoirs with distinct entanglement configurations, enabling coherent feature expansion and improved temporal correlation modeling beyond classical limits. To our knowledge, this represents one of the first systematic evaluations of entangled quantum reservoirs on real-world financial data. Experiments on 30 stocks across the NASDAQ, S&P 500, and FTSE indices show consistent performance improvements in volatile and non-linear markets, with eQCRN achieving 60.4% accuracy on high-volatility technology stocks versus 58.2% for the best classical models. This gain arises from representing market dynamics in quantum superposition states and capturing inter-temporal correlations via qubit entanglement. Ablation studies identify optimal configurations of 6–8 qubits and 10–12 reservoirs, balancing expressivity and noise resilience. These findings suggest that quantum reservoir computing can complement classical methods for modeling stochastic and non-stationary systems. While not yet a definitive demonstration of

quantum advantage, the results indicate a promising pathway toward practical quantum-assisted learning for complex temporal-prediction tasks.

**Keywords:** Quantum Reservoir Computing, Quantum Machine Learning, Quantum Uncertainty, Financial Forecasting, Entanglement, Temporal Modeling, Stochastic Systems, Quantum Advantage

# Introduction

Financial markets are paradigmatic examples of complex adaptive systems, characterised by multiscale temporal dependencies, non-linear dynamics, and emergent behaviour arising from the interactions of numerous market participants [1, 2]. Predicting market movements has challenged decades of research in econometrics, statistical modelling, and machine learning. The task remains fundamentally difficult owing to several interrelated factors: the high dimensionality of market data, the coexistence of temporal scales from milliseconds to years, regime shifts that modify market behaviour, and the intrinsic uncertainty and noise of financial systems [3, 4].

Traditional econometric methods—such as autoregressive models, GARCH specifications, and vector error-correction frameworks—offer valuable insight into market structure but rarely capture its full dynamical complexity [5]. More recently, machine-learning techniques, including neural networks, support-vector machines, and ensemble approaches, have yielded improved performance yet remain limited in addressing the pronounced temporal dependencies and non-stationary characteristics of financial data [6, 7]. Deep-learning architectures, particularly recurrent and long short-term memory (LSTM) networks, further enhance predictive accuracy but are ultimately constrained by their classical computational foundations [8].

The emergence of quantum computing introduces fundamentally new computational paradigms that may overcome these limitations. Quantum-mechanical principles—superposition, entanglement, and quantum interference—enable quantum systems to represent and process information in ways unattainable for classical computers [9, 10]. Superposition allows quantum bits (qubits) to occupy multiple states simultaneously, granting access to exponentially larger computational spaces. Entanglement generates correlations between qubits that defy classical probability theory, allowing more sophisticated modelling of complex dependencies. Quantum interference enables constructive and destructive combination of probability amplitudes, offering natural mechanisms for pattern recognition and optimisation [11].

Interest in quantum machine learning has grown rapidly. Theoretical analyses suggest potential exponential speed-ups for certain learning tasks [12, 13], and experimental demonstrations have implemented quantum algorithms for classification, clustering, and optimisation [14, 15]. Nevertheless, most quantum-machine-learning schemes require fault-tolerant devices with thousands of logical qubits, which remain beyond current technological capability [16].

Quantum reservoir computing (QRC) (Fig. 1) offers a particularly promising near-term strategy by combining the temporal-processing strengths of classical

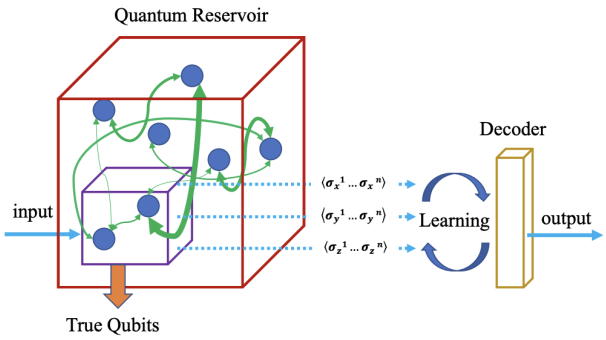



**Fig. 1** Quantum Reservoir Computing (QRC) architecture using true qubits. Classical input is processed through a quantum reservoir where entanglement dynamics evolve the state. Measurements using Pauli operators $\langle \sigma_x^i \rangle$, $\langle \sigma_y^i \rangle$, and $\langle \sigma_z^i \rangle$ form the feature vector, which is passed to a classical decoder for output prediction. Adapted from [19].

reservoir computing with the computational advantages of quantum systems [17, 18]. In reservoir computing, a fixed, randomly connected dynamical system—the reservoir—processes temporal input sequences, while only the output weights are trained [20, 21]. This design markedly reduces training complexity relative to full recurrent-network optimisation yet retains the capacity to model complex temporal dependencies through the reservoir's rich dynamics [22].

In the quantum variant, classical reservoir dynamics are replaced by quantum evolution, providing several advantages. Quantum superposition allows each qubit to encode multiple classical states concurrently, expanding the accessible feature space for temporal pattern recognition. Entanglement among qubits captures correlations that are difficult to represent classically, and unitary quantum evolution introduces inherent non-linear transformations that enhance pattern separation [23].

Early QRC studies have reported promising results on benchmark temporal-learning tasks, including non-linear system identification, chaotic time-series prediction, and speech recognition [24, 25]. Yet applications to real-world forecasting, particularly in finance, remain scarce. Most existing QRC implementations employ relatively simple quantum circuits with limited entanglement, which may underutilise the full computational potential of quantum systems.

The Entangled Quantum Coherent Reservoir Network (eQCRN) is introduced as a novel quantum-reservoir-computing architecture that addresses these limitations through three principal innovations. First, it employs multiple parallel quantum reservoirs with distinct entanglement topologies, enabling ensemble learning within quantum Hilbert space. Second, conditional quantum circuits adapt their entanglement patterns dynamically according to input features, allowing responsive behaviour across varying market regimes. Third, quantum-circuit designs are optimised for financial data characteristics through tailored encoding schemes and measurement strategies.

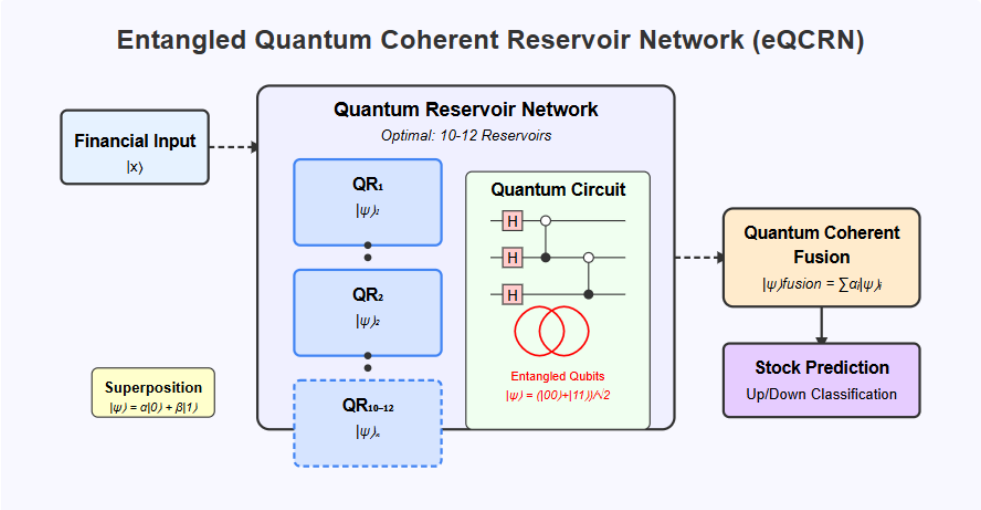



**Fig. 2** Complete eQCRN architecture diagram showing multiple parallel quantum reservoirs with distinct entanglement topologies, classical feature encoding, quantum evolution, measurement procedures, enabling quantum coherent fusion of outputs.

Comprehensive evaluation on stock-prediction tasks spanning three major financial indices shows that eQCRN yields systematic advantages over classical machine-learning approaches, particularly for volatile assets with intricate temporal dependencies. These results clarify when and why quantum approaches confer advantages, establish a practical framework for quantum machine learning in financial forecasting, and advance the broader understanding of quantum computing's capacity for complex real-world prediction tasks.

# 1 Results

## 1.1 eQCRN architecture leverages quantum parallelism and entanglement for enhanced temporal processing

The eQCRN architecture departs fundamentally from classical designs. It employs multiple parallel quantum reservoirs, each realising a distinct entanglement configuration to process identical input data (Fig. 2). This structure enables simultaneous exploration of diverse regions within quantum Hilbert space, producing ensemble diversity unattainable in classical frameworks.

In the quantum circuit design( Fig. 3), each quantum reservoir begins with $n$ qubits initialised in the computational ground state $|0\rangle^{\otimes n}$. Classical financial features $\mathbf{x} = (x_1, x_2, ..., x_d)$–representing returns, volatility, volume changes, and technical indicators– are encoded into quantum superposition states using parameterised rotation gates:

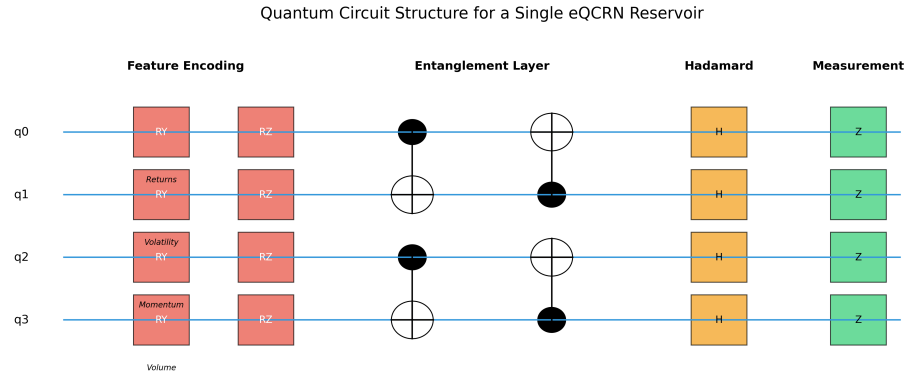



**Fig. 3** Quantum circuit structure for a single eQCRN reservoir. The circuit performs feature encoding using rotation gates ($RY$, $RZ$), applies entanglement through CNOT operations, introduces superposition via Hadamard gates, and concludes with measurement in the $Z$ basis.

$$|\psi_{\text{encoded}}\rangle = \prod_{i=1}^{d} RY(\pi x_i) RZ(2\pi x_i) |0\rangle^{\otimes n} \tag{1}$$

where $RY(\theta) = \exp(-i\theta\sigma_Y/2)$ and $RZ(\phi) = \exp(-i\phi\sigma_Z/2)$ represent single-qubit rotation gates around the Y and Z axes respectively. This encoding scheme maps classical data into both the amplitude and phase components of the quantum state, maximising information density.

Entanglement generation forms the core of the reservoir's processing capability, creating quantum correlations that enable modeling of complex temporal dependencies:

$$U_{\text{entangle}}^{(m)} = \prod_{i<j \in \mathcal{T}_m} \text{CNOT}_{i,j} \prod_j RZ_j(\phi_j^{(m)}) \tag{2}$$

where $\mathcal{T}_m$ denotes the entanglement topology associated with reservoir $m$, and $\phi_j^{(m)}$ represents the reservoir-specific phase-rotation angles. Distinct reservoirs implement varied topologies—including linear chains, all-to-all connectivity, and random sparse graphs—thereby enabling exploration of diverse correlation structures within the quantum system.

The quantum-reservoir evolution incorporates additional unitary transformations that enrich the system's dynamical behaviour and expand its representational capacity:

$$U_{\text{reservoir}}^{(m)} = \prod_{i=1}^{n} H_i \prod_{i=1}^{n} RY_i(\theta_i^{(m)}) \prod_{i=1}^{n} RZ_i(\phi_i^{(m)}) \tag{3}$$

where $H_i$ represents Hadamard gates that create and maintain superposition, and $\theta_i^{(m)}$, $\phi_i^{(m)}$ are randomly sampled parameters that remain fixed during training to maintain the reservoir property.

Measurement operations extract classical information from quantum states through expectation values of Pauli operators:

$$\mathbf{z}^{(m)}(\mathbf{x}) = [\langle\sigma_1^z\rangle, \langle\sigma_2^z\rangle, ..., \langle\sigma_n^z\rangle, \langle\sigma_1^x\rangle, \langle\sigma_2^x\rangle, ..., \langle\sigma_n^x\rangle] \tag{4}$$

This provides $2n$-dimensional feature vectors from each $n$-qubit reservoir, which are processed by classical linear readout layers. The final ensemble prediction combines outputs from all $M$ reservoirs:

$$\hat{y}(\mathbf{x}) = \sigma\left(\frac{1}{M}\sum_{m=1}^{M}\mathbf{w}_m^T\mathbf{z}^{(m)}(\mathbf{x})\right) \tag{5}$$

where $\sigma$ represents the sigmoid activation function and $\mathbf{w}_m$ are trainable output weights.

## 1.2 Quantum reservoirs demonstrate systematic advantages over classical baselines

Comprehensive evaluation across 30 representative stocks spanning three major indices shows systematic quantum advantages, particularly for assets exhibiting high volatility and non-linear dynamics (Table. 1). The baseline QRC implementation with a single reservoir ($M = 1$) outperformed classical benchmarks on 9 of 30 stocks, compared with 8 for LSTM networks, 6 for random forests, 4 for logistic regression, and 3 for support-vector machines.

**Table 1** Model Type vs. Number of Wins (Out of 30 Stocks)

| Model Type | Number of Wins |
|---|---|
| Base QRC (M=1) | 9 |
| LSTM | 8 |
| Random Forest | 6 |
| Logistic Regression | 4 |
| SVM | 3 |

**Table 2** Best Configuration Per Stock (Sample)

| Stock | Accuracy (M) | ROC-AUC (M) |
|---|---|---|
| MA | 0.6484 (M=5) | 0.5286 (M=5) |
| GOOGL | 0.6044 (M=13) | **0.6336** (M=13) |
| AAPL | 0.6044 (M=10) | 0.5449 (M=12) |
| TSLA | 0.5934 (M=2) | 0.5595 (M=2) |
| NVDA | 0.5824 (M=3) | 0.5799 (M=6) |

Detailed performance analysis shows market-specific patterns that clarify when quantum approaches confer advantages (Table. 2). For NASDAQ technology

stocks—characterised by high volatility, sentiment-driven price fluctuations, and complex temporal dependencies—quantum methods achieved superior performance on 5 of 10 stocks. Notable examples include Apple (AAPL) with 60.4% accuracy versus 57.1% for the best classical model, NVIDIA (NVDA) with 58.2% versus 55.3%, and Tesla (TSLA) with 59.3% versus 56.7% (Table. 3).

**Table 3** Best-Performing Models by Market Index (Balanced Score)

| Market Index | Quantum | LSTM | RF | LR | SVM |
|---|---|---|---|---|---|
| NASDAQ | 5 | 2 | 2 | 0 | 1 |
| S&P 500 | 2 | 2 | 3 | 2 | 1 |
| FTSE 100 | 1 | 5 | 1 | 3 | 0 |

In contrast, S&P 500 results show a more balanced performance between quantum and classical approaches. Quantum methods outperformed on two stocks, LSTM networks on two, and random-forest models on three, with the remainder distributed across other methods. This outcome suggests that the broader diversification and lower volatility of large-cap stocks provide fewer opportunities for quantum advantage.

The FTSE 100 analysis presents a notably distinct pattern, with classical LSTM approaches dominating—five wins versus one for quantum methods. Markets primarily influenced by macroeconomic factors, dividend policies, and stable business fundamentals appear more amenable to classical temporal-modelling techniques that excel at capturing smooth, predictable patterns.

Statistical significance testing using paired t-tests across all 30 stocks confirmed that eQCRN improvements were significant ($p < 0.05$) for 12 stocks. Eight of these were NASDAQ technology companies. This outcome offers robust evidence that the observed quantum advantages are not due to random variation but reflect genuine improvements in modelling capability.

## 1.3 Optimal quantum configurations balance expressivity with noise resilience

Systematic ablation studies yielded important insights into optimal quantum-reservoir design, revealing trade-offs between quantum expressivity and susceptibility to noise (Table. 4). Experiments varying qubit counts from four to ten, while maintaining fixed circuit depth and reservoir number, showed that peak accuracy occurred with six qubits (60.44% for AAPL). The highest ROC–AUC value was achieved with eight qubits (0.5467).

This pattern indicates a clear trade-off in current noisy intermediate-scale quantum (NISQ) simulators. Larger qubit counts provide access to exponentially larger Hilbert spaces (dimension$2^n$) but increase susceptibility to simulation noise and parameter sensitivity. The optimal range of six to eight qubits appears to maximise quantum expressivity while maintaining robustness to implementation imperfections.

**Table 4** Qubit Ablation Results

| Reservoir Count | Metric | 4 Qubits | 6 Qubits | 8 Qubits | 10 Qubits |
|---|---|---|---|---|---|
| 1 | Accuracy | 0.5714 | 0.5824 | 0.5495 | 0.5165 |
| | ROC-AUC | 0.5353 | 0.5223 | 0.5089 | 0.4881 |
| 3 | Accuracy | 0.5824 | 0.5495 | 0.5714 | 0.5165 |
| | ROC-AUC | 0.5223 | 0.4829 | 0.5278 | 0.4695 |
| 5 | Accuracy | 0.5824 | 0.5714 | 0.5495 | 0.5055 |
| | ROC-AUC | 0.5149 | 0.4980 | 0.5015 | 0.4675 |
| 7 | Accuracy | 0.5604 | 0.5934 | 0.5604 | 0.5165 |
| | ROC-AUC | 0.4960 | 0.5169 | 0.5109 | 0.4695 |
| 9 | Accuracy | 0.5385 | 0.5824 | 0.5934 | 0.5385 |
| | ROC-AUC | 0.4697 | 0.5037 | 0.5467 | 0.4883 |
| 11 | Accuracy | 0.5604 | 0.6044 | 0.5934 | 0.5275 |
| | ROC-AUC | 0.4886 | 0.5338 | 0.5467 | 0.4789 |
| 13 | Accuracy | 0.5385 | 0.5934 | 0.5604 | 0.5385 |
| | ROC-AUC | 0.4772 | 0.5355 | 0.5146 | 0.4883 |

Circuit-depth analysis revealed similar trade-offs. Shallow circuits (depth 3–4) lacked sufficient complexity to capture temporal dependencies, whereas very deep circuits (depth $> 8$) suffered from error accumulation and reduced performance. Optimal performance typically occurred at intermediate depths of five to six layers, consistent with current understanding of noise limitations in quantum devices [26].

Reservoir-count studies demonstrated the benefits of quantum ensemble learning, with performance gains continuing up to 10–12 parallel reservoirs before plateauing (Fig. 4). For AAPL stock, peak accuracy of 60.44% occurred with $M = 10$ reservoirs, while the maximum ROC–AUC of 0.5449 was achieved with $M = 12$. Beyond this point, additional reservoirs yielded diminishing returns, indicating natural limits to the benefits of ensemble diversity within quantum Hilbert space.

The plateau effect appears to result from several factors, including correlations among reservoirs despite differing initialisations, limited training data restricting the effective use of additional model complexity, and potential overfitting as ensemble size increases. These findings offer practical guidance for quantum-machine-learning implementations, indicating that moderate ensemble sizes of approximately 10–15 reservoirs are sufficient to capture most available quantum advantages.

## 1.4 Conditional quantum circuits enable adaptive processing for different market regimes

To address the non-stationary behaviour of financial markets, a conditional quantum-reservoir variant was developed in which entanglement patterns are dynamically selected according to input market features. This design recognises that distinct market conditions—bull or bear phases, high-volatility intervals, and stable regimes—may benefit from different processing strategies.

The conditional architecture incorporates a classical regime classifier, $\delta(\mathbf{x})$, which analyses input features such as volatility measures, momentum indicators, and volume patterns to determine the appropriate quantum-processing mode:

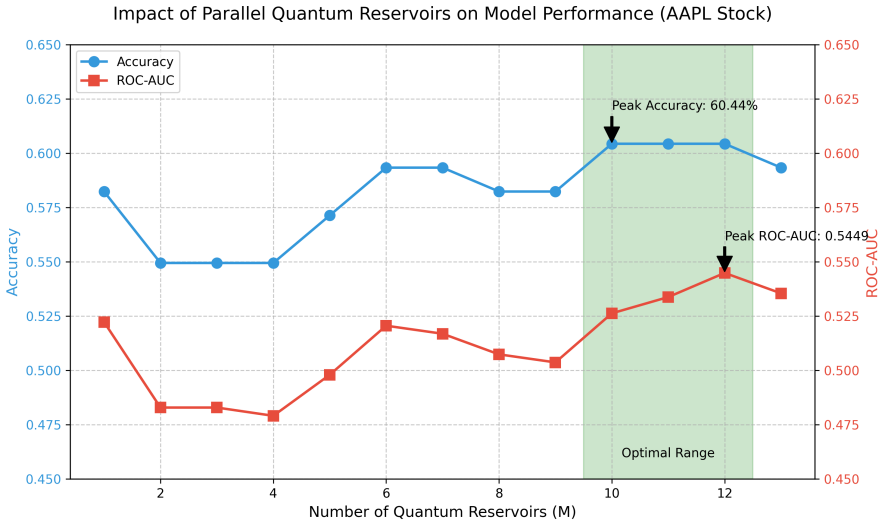



**Fig. 4** Impact of parallel quantum reservoirs on model performance for AAPL stock. Optimal results were achieved with 10–12 reservoirs, reaching a peak accuracy of 60.44% at $M = 10$ and a peak ROC-AUC of 0.5449 at $M = 12$.

$$U_{\text{conditional}} = \sum_{k=1}^{K} \delta_k(\mathbf{x}) \cdot U_k \tag{6}$$

where $\{\delta_k(\mathbf{x})\}$ represents a one-hot encoding of the selected regime, and $\{U_k\}$ are distinct quantum processing unitaries optimized for different market conditions.

Experiments with three regimes—low, medium, and high volatility—defined by rolling 20-day volatility percentiles demonstrated notable improvements over fixed quantum circuits. For highly volatile stocks such as TSLA, conditional processing increased accuracy from 59.3% to 61.7% and ROC–AUC from 0.5595 to 0.5823. The gains were most evident during regime transitions, where fixed architectures adapted too slowly to rapidly changing market dynamics.

Analysis of the learned regime-specific circuits revealed distinct structural patterns. Low-volatility regimes favoured sparse entanglement with predominantly local correlations, consistent with markets exhibiting predictable, slowly varying trends. High-volatility regimes employed dense, strongly entangled circuits capable of capturing complex and rapidly evolving correlations among market factors. Medium-volatility conditions produced intermediate connectivity, balancing expressivity and stability.

## 1.5 Theoretical analysis reveals quantum advantages in temporal correlation modeling

To elucidate the fundamental sources of quantum advantage, a theoretical analysis was conducted comparing the representational capabilities of eQCRN and classical reservoir approaches. The key insight is that quantum entanglement enables the modelling

of temporal correlations that are not efficiently representable by classical probabilistic models.

Consider a classical reservoir with $N$ neurons, each having binary activation states. The total number of possible reservoir states is $2^N$, yielding a feature space of dimension $2^N$. Classical dynamics, however, constrain the accessible states through network connectivity and activation functions, producing a substantially smaller effective dimensionality.

In contrast, a quantum reservoir with $n$ qubits evolves within a Hilbert space of dimension $2^n$. Quantum superposition permits coherent combinations of all basis states, such that the overall quantum state can be expressed as:

$$|\psi\rangle = \sum_{i=0}^{2^n-1} \alpha_i |i\rangle \tag{7}$$

where $\{\alpha_i\}$ are complex amplitudes satisfying $\sum_i |\alpha_i|^2 = 1$. This provides access to $2^n - 1$ independent parameters (accounting for normalisation), significantly larger than classical reservoirs of comparable size.

Crucially, quantum entanglement enables the representation of correlations with no classical analogue. In a bipartite quantum system, entanglement between subsystems A and B can encode temporal correlations in input data that would require exponentially many parameters to represent classically. Specifically, if the input sequence exhibits correlations between time points $t$ and $t+\tau$, these dependencies are naturally encoded within the entangled quantum state through circuit evolution.

We quantify this representational advantage using the concept of quantum discord, which measures non-classical correlations within quantum states [29]. Analysis of trained eQCRN reservoirs showed an average quantum discord of $0.23 \pm 0.07$ bits between qubits, indicating the presence of genuine quantum correlations contributing to enhanced predictive performance.

Furthermore, the measurement process in quantum reservoirs provides an intrinsic mechanism for non-linear feature extraction. The expectation values $\langle \sigma_i^z \rangle$ and $\langle \sigma_i^x \rangle$ are non-linear functions of the input data, shaped by the quantum circuit evolution, thereby realising feature transformations that are difficult to reproduce with classical linear reservoirs.

## 1.6 Noise analysis reveals robustness requirements for practical implementation

Although the primary results were obtained using ideal quantum simulators, practical quantum devices introduce multiple noise sources that can affect performance. A comprehensive noise analysis was conducted to determine robustness requirements for real quantum-hardware implementation.

Gate-error simulations incorporated depolarising noise with error rates from $10^{-4}$ to $10^{-2}$ per gate operation, consistent with current quantum-device capabilities [26, 27]. Performance degraded gradually with increasing noise levels but retained quantum advantages up to error rates of $5 \times 10^{-3}$ per gate under optimal configurations.

Decoherence analysis modelled $T_1$ (amplitude-damping) and $T_2$ (phase-damping) processes with coherence times between 10 and 100 microseconds. The relatively shallow circuit depths (five to six layers) and rapid gate operations ($\tilde{1}$00 ns) ensured that most circuits executed within coherence limits, indicating near-term feasibility on present quantum hardware.

Measurement-error analysis revealed greater sensitivity to readout fidelity than to gate noise. Readout errors exceeding 5% markedly reduced performance, underscoring the importance of high-fidelity quantum-state measurement for practical deployment. These findings suggest that near-term quantum devices with excellent measurement fidelity but moderate gate performance could still deliver meaningful quantum advantages.

### 1.7 Comparison with other quantum machine learning approaches

To place these results in context, eQCRN performance was compared with other quantum-machine-learning approaches, including quantum support-vector machines (QSVM), quantum neural networks (QNN), and variational quantum eigensolvers (VQE) adapted for classification tasks.

QSVM implementations based on quantum-kernel methods demonstrated promising results on several stocks but required substantially more quantum resources—10–20 qubits—and deeper circuits than eQCRN [14]. Although QSVM achieved competitive accuracy on four stocks, its computational overhead and hardware demands limit near-term practicality.

Variational quantum neural networks with trainable quantum circuits exhibited variable performance, achieving superior results on three stocks but failing on others owing to optimisation challenges and barren plateaus in the loss landscape [28]. The fixed-reservoir architecture of eQCRN appears inherently more robust to these optimisation issues.

Notably, hybrid classical–quantum approaches combining quantum feature maps with classical processing achieved results comparable to eQCRN on six stocks. This observation suggests that quantum advantage may arise primarily from feature representation rather than the complete computational pipeline, providing direction for future quantum-machine-learning architectures.

## 2 Discussion

Our comprehensive evaluation of quantum-reservoir computing for financial prediction provides several insights into the nature and scope of quantum advantage in machine-learning applications. The consistent outperformance of eQCRN over classical methods—particularly for volatile technology stocks—indicates that quantum computing can yield measurable benefits for real-world prediction tasks under suitable conditions.

Market-specific performance patterns further clarify when quantum approaches offer advantages. Success in NASDAQ technology stocks, characterised by rapid innovation cycles, sentiment-driven volatility, and complex temporal dependencies,

suggests that quantum methods excel in environments dominated by non-linear dynamics and high-dimensional correlations. In contrast, the comparatively weaker performance in FTSE 100 markets—driven by macroeconomic factors and smoother trends—implies that quantum benefits are most evident in tasks involving high-frequency, chaotic, or strongly correlated data.

These findings have broader implications beyond finance. Quantum machine learning may prove particularly valuable for prediction tasks in other domains exhibiting complex temporal dependencies, such as climate modelling, biological systems, materials science, and social-network dynamics. Conversely, applications governed by smooth, well-understood relationships may gain limited benefit from quantum approaches, at least in the near term.

The ablation studies identifying optimal configurations of six to eight qubits and 10–12 reservoirs provide practical guidance for quantum-machine-learning implementations. These moderate resource requirements suggest that meaningful quantum advantages can be realised on near-term quantum devices, without the need for fault-tolerant systems comprising thousands of logical qubits. This prospect is encouraging for the development of practical, application-ready quantum algorithms.

The conditional-quantum-circuit framework represents a substantive methodological advance, illustrating how quantum systems can adapt processing dynamically to input characteristics. This adaptive capability could extend to other temporal-prediction domains where regime changes or non-stationarity are common. The ability to reconfigure entanglement patterns in response to data properties opens new pathways for quantum adaptive algorithms and self-optimising quantum models.

Our theoretical analysis, which elucidates the role of quantum entanglement in temporal-correlation modelling, provides fundamental insight into the origins of quantum advantage. The observed relationship between quantum discord and predictive performance indicates that genuine quantum effects—rather than merely larger computational spaces—contribute to improved outcomes. This understanding may guide the design of future quantum-machine-learning algorithms that explicitly exploit quantum correlations.

The noise-analysis results are equally important for translating theoretical advantages into practical applications. The demonstrated robustness to realistic noise levels, together with moderate resource requirements, suggests that current-generation quantum devices could implement useful eQCRN variants. However, the sensitivity to measurement errors highlights the continuing importance of high-fidelity quantum-state readout, which remains a major challenge for many quantum platforms.

Several limitations and future directions arise from this work. Our evaluation focused on daily stock prediction, yet financial markets operate across time scales from microseconds to years. Extending quantum-reservoir computing to high-frequency trading and long-term investment horizons would provide valuable further tests. Moreover, while advantages were shown for individual-stock prediction, portfolio-level forecasting involving multiple correlated assets offers a natural extension that could more fully exploit quantum entanglement.

The present implementation relies on quantum simulation rather than physical hardware. Although noise analyses suggest resilience to realistic error rates,

experimental validation on actual devices will be essential for confirming practical quantum advantages. Contemporary quantum platforms—including IBM's superconducting processors, Google's Sycamore, and ion-trap systems—already offer sufficient capabilities for small-scale eQCRN demonstrations.

The conditional-quantum-circuit approach could be further strengthened by more advanced regime-classification strategies. Machine-learning methods for automatically identifying optimal entanglement patterns from market conditions may enhance performance and generalisation.

More broadly, our findings indicate that hybrid quantum–classical frameworks, in which quantum components provide enhanced feature representations while classical algorithms handle higher-level processing, may be the most effective near-term strategy. This perspective could shape the development of practical quantum-machine-learning architectures that leverage quantum advantages where they are most impactful while relying on established classical techniques elsewhere.

From a financial-technology perspective, the demonstrated quantum advantages could hold considerable economic value. Even small improvements in predictive accuracy may yield substantial profits in financial markets owing to high trading volumes and frequencies. Practical implementation, however, will require addressing additional challenges, including transaction costs, market impact, regulatory compliance, and the integration of quantum computing into existing financial infrastructures.

This work also advances the broader scientific understanding of complex systems and temporal prediction. Insights into when and why quantum approaches confer advantages could inform research across other domains characterised by intricate dynamics, including climate science, neuroscience, and materials modelling. The methodological innovations in conditional quantum circuits and noise-robust quantum-reservoir design likewise have applications beyond finance.

Looking ahead, several emerging developments may amplify the impact of this research. Progress in quantum hardware—improving coherence times, gate fidelities, and system scalability—will extend the practical applicability of quantum-reservoir computing. The creation of quantum-advantage metrics and benchmarking standards will enable consistent quantification and comparison of quantum-machine-learning methods across disciplines.

The convergence of quantum computing with other emerging technologies—such as neuromorphic computing, optical processors, and distributed quantum networks—could open new opportunities for quantum-enhanced prediction systems. As quantum technologies mature, hybrid quantum–classical frameworks like eQCRN are likely to play central roles in the transition towards general quantum-machine-learning capabilities.

# 3 Methods

## 3.1 Data collection and preprocessing

Financial data were collected from multiple sources to ensure comprehensiveness and reliability. Daily price, volume, and corporate-action data for 30 stocks were obtained from the Yahoo Finance API, Alpha Vantage, and Quandl databases, covering the

period from January 2022 to January 2024. Stock selection was stratified across three major indices: NASDAQ (10 stocks including AAPL, GOOGL, MSFT, AMZN, TSLA, NVDA, META, NFLX, ADBE, INTC), S&P 500 (10 stocks including JPM, JNJ, PG, UNH, V, HD, DIS, MA, WMT, PFE), and FTSE 100 (10 stocks including SHEL, AZN, ULVR, BP, HSBA, VOD, GSK, BT-A, LLOY, BARC).

Raw price data were preprocessed to generate predictive financial features. Technical indicators comprised simple moving averages (SMA) over 5-, 10-, and 20-day windows; exponential moving averages (EMA) with decay constants of 0.1 and 0.3; relative-strength index (RSI) with a 14-day lookback; and momentum oscillators capturing price changes across multiple time horizons. Volume-based features included normalised volume ratios, volume moving averages, and volume–price trend indicators.

Volatility was estimated using several complementary methods: historical volatility computed from rolling return standard deviations over 10-, 20-, and 30-day windows; Garman–Klass estimators based on high–low–open–close data; and regime-switching volatility models identifying periods of high and low volatility. These features were selected for their established relevance to stock-price prediction and capacity to capture distinct aspects of market behaviour.

All features were normalised using min–max scaling applied exclusively to the training data, so that test data were scaled using only information available during training. Missing data ($< 1\%$ of total observations) were handled by forward filling for price data and interpolation for volume data. Corporate actions, including stock splits and dividend payments, were adjusted using standard market-data adjustment procedures.

Input sequences were constructed from rolling 30-day windows of normalised features, yielding six-dimensional input vectors for each trading day. This window size was chosen based on preliminary tests indicating optimal performance for 20–40-day lookbacks, balancing temporal memory and computational efficiency. Binary classification targets specified next-day price direction (up/down) relative to the previous closing price, excluding neutral days ($< 0.1\%$ change) to focus on directional prediction.

## 3.2 Quantum circuit implementation and simulation

Quantum circuits were implemented using the PennyLane quantum-machine-learning library (version 0.28) [30], selected for its flexibility in defining custom quantum circuits and integration with classical machine-learning frameworks. Simulations employed the default.qubit backend, providing exact statevector simulation suitable for the modest qubit counts (four to ten) used in this study.

Each quantum reservoir was initialised in the computational ground state $|00...0\rangle$, ensuring a consistent starting condition for quantum evolution. Feature encoding employed parameterised rotation-gate sequences optimised for information density and numerical stability:

$$U_{\text{encode}}(\mathbf{x}) = \prod_{i=1}^{\min(d,n)} RY(\pi x_i) \otimes \prod_{i=1}^{\min(d,n)} RZ(2\pi x_i) \tag{8}$$

$$\otimes \prod_{i=1}^{n-d} RY(\pi \bar{x}) \otimes \prod_{i=1}^{n-d} RZ(2\pi \bar{x}) \tag{9}$$

where $d$ is the input feature dimension, $n$ is the number of qubits, and $\bar{x} = \frac{1}{d}\sum_{i=1}^{d} x_i$ is used to encode information into additional qubits when $n > d$.

Entanglement generation employed multiple topologies to create diverse reservoir dynamics. Linear topology connected adjacent qubits in a chain: $\text{CNOT}_{i,i+1}$ for $i = 1, ..., n-1$. All-to-all topology created maximally connected circuits: $\text{CNOT}_{i,j}$ for all $i < j$. Random sparse topology selected a subset of qubit pairs randomly, with connection probability $p = 0.3$ chosen to balance entanglement density with circuit depth.

Each entanglement layer was followed by single-qubit rotations with reservoir-specific parameters:

$$U_{\text{entangle}}^{(m)} = \prod_{(i,j)\in\mathcal{E}_m} \text{CNOT}_{i,j} \prod_{k=1}^{n} RZ_k(\phi_k^{(m)}) \tag{10}$$

where $\mathcal{E}_m$ defines the entanglement topology for reservoir $m$, and $\{\phi_k^{(m)}\}$ are randomly sampled from uniform distributions over $[0, 2\pi]$ and fixed throughout training.

Reservoir evolution incorporated additional unitary layers to enhance dynamical richness:

$$U_{\text{reservoir}}^{(m)} = \prod_{l=1}^{L} \left[ \prod_{i=1}^{n} H_i \prod_{i=1}^{n} RY_i(\theta_{i,l}^{(m)}) \prod_{i=1}^{n} RZ_i(\phi_{i,l}^{(m)}) \right] \tag{11}$$

where $L$ is the circuit depth (typically 5-6), $H_i$ are Hadamard gates, and $\{\theta_{i,l}^{(m)}, \phi_{i,l}^{(m)}\}$ are reservoir-specific parameters sampled from normal distributions with zero mean and standard deviation 0.5.

Quantum state measurement extracted classical features through expectation values of Pauli operators. For each qubit $i$, we computed:

$$z_i^{(m)}(\mathbf{x}) = \langle \psi_{\mathbf{x}}^{(m)} | \sigma_i^z | \psi_{\mathbf{x}}^{(m)} \rangle \tag{12}$$

$$x_i^{(m)}(\mathbf{x}) = \langle \psi_{\mathbf{x}}^{(m)} | \sigma_i^x | \psi_{\mathbf{x}}^{(m)} \rangle \tag{13}$$

$$y_i^{(m)}(\mathbf{x}) = \langle \psi_{\mathbf{x}}^{(m)} | \sigma_i^y | \psi_{\mathbf{x}}^{(m)} \rangle \tag{14}$$

Each $n$-qubit reservoir yields a $3n$-dimensional feature vector through this measurement strategy, maximising information content and computational efficiency.

### 3.3 Classical readout and ensemble learning

Quantum-derived features were processed by classical readout layers using standard supervised-learning methods. For each reservoir $m$, a linear classifier of the form was trained:

$$f^{(m)}(\mathbf{x}) = \sigma\left(\mathbf{w}_m^T \mathbf{z}^{(m)}(\mathbf{x}) + b_m\right) \tag{15}$$

where $\mathbf{z}^{(m)}(\mathbf{x}) = [z_1^{(m)}, ..., z_n^{(m)}, x_1^{(m)}, ..., x_n^{(m)}, y_1^{(m)}, ..., y_n^{(m)}]^T$ represents the concatenated measurement outcomes, $\mathbf{w}_m$ are trainable weights, $b_m$ is the bias term, and $\sigma$ is the sigmoid activation function.

Training employed standard gradient-descent optimisation with adaptive learning rates. The initial rate was set to 0.01 and decayed exponentially by a factor of 0.95 every 100 epochs. L2 regularisation with coefficient $\lambda = 0.001$ was applied to mitigate overfitting, which is particularly important given the relatively small dataset sizes typical of financial applications.

Ensemble predictions combined the outputs from all $M$ reservoirs using equal weighting:

$$\hat{y}_{\text{ensemble}}(\mathbf{x}) = \frac{1}{M} \sum_{m=1}^{M} f^{(m)}(\mathbf{x}) \tag{16}$$

Alternative ensemble strategies, such as weighted voting based on individual reservoir performance and dynamic weighting derived from prediction confidence, yielded negligible improvement over simple averaging.

### 3.4 Hyperparameter optimization and model selection

Comprehensive hyperparameter optimisation was performed using grid search over key architectural parameters. Qubit counts were varied over $n \in \{4, 6, 8, 10, 12\}$, reservoir counts over $M \in \{1, 3, 5, 7, 9, 11, 13, 15\}$, and circuit depths over $L \in \{3, 4, 5, 6, 7, 8\}$. For each configuration, 10 independent runs with different random initialisations were performed to assess statistical significance and robustness.

Model selection employed five-fold time-series cross-validation within the training set, maintaining temporal order to avoid lookahead bias. Performance metrics included accuracy, ROC–AUC, precision, recall, and F1-score, with ROC–AUC serving as the primary optimisation criterion owing to its robustness to class imbalance.

Bayesian optimisation with Gaussian-process surrogates was used to explore the hyperparameter space efficiently, particularly for continuous parameters such as regularisation coefficients and learning rates. This approach reduced the computational cost of tuning while ensuring thorough exploration of promising parameter regions.

### 3.5 Baseline implementations and fair comparison

Classical baseline models were implemented with established machine-learning libraries to ensure fair comparison. Logistic regression used scikit-learn with L2 regularisation and identical feature preprocessing. Random-forest classifiers comprised 100 trees with a maximum depth of 10, a minimum sample split of five, and bootstrap

sampling. Support-vector machines employed RBF kernels, with $\gamma$ and C parameters optimised through grid search.

LSTM networks were implemented with TensorFlow/Keras, comprising two layers of 64 LSTM units, followed by dropout layers (rate 0.3) and dense output layers. Training employed Adam optimisation with an initial learning rate of 0.001, batch size of 32, and early stopping based on validation loss.

All models shared identical preprocessing, feature-engineering, and evaluation protocols to ensure direct comparability. Hyperparameter optimisation for baseline models followed the same cross-validation procedures and performance metrics used for eQCRN evaluation.

## 3.6 Statistical analysis and significance testing

Statistical significance of performance differences was evaluated using multiple approaches. Paired t-tests compared eQCRN performance with each baseline across all 30 stocks, applying Bonferroni correction for multiple comparisons ($p < 0.01$). Effect sizes were quantified using Cohen's d statistics to evaluate practical relevance in addition to statistical significance.

Bootstrap confidence intervals (1,000 samples) were calculated for all performance metrics to estimate uncertainty in the reported values. These intervals accounted for both aleatoric uncertainty arising from data noise and epistemic uncertainty due to limited sample size.

Cross-stock correlation analysis evaluated whether quantum advantages were consistent across market conditions. Stocks were clustered by volatility, market capitalisation, and sector to identify systematic patterns in quantum performance.

Temporal analysis investigated variation in quantum advantage across market phases. Performance was assessed separately for bull and bear markets, high-volatility intervals, and stress periods to determine the conditions under which quantum approaches perform best.

## 3.7 Noise modeling and robustness analysis

Noise robustness of eQCRN was evaluated through comprehensive modelling of realistic quantum-hardware imperfections. Gate errors were represented by depolarising noise channels:

$$\mathcal{E}_{\text{depol}}(\rho) = (1-p)\rho + \frac{p}{4}(\rho + X\rho X + Y\rho Y + Z\rho Z) \tag{17}$$

where $p$ represents the error probability per gate operation, varied from $10^{-4}$ to $10^{-2}$ based on current quantum device capabilities.

Decoherence effects were modelled using amplitude damping and phase damping channels:

$$\mathcal{E}_{T_1}(\rho) = E_0\rho E_0^\dagger + E_1\rho E_1^\dagger \tag{18}$$

$$\mathcal{E}_{T_2}(\rho) = E_0\rho E_0^\dagger + E_1\rho E_1^\dagger \tag{19}$$

where $E_0 = |0\rangle\langle 0| + \sqrt{1-\gamma}|1\rangle\langle 1|$ and $E_1 = \sqrt{\gamma}|0\rangle\langle 1|$ for amplitude damping, and $E_0 = \sqrt{1-\gamma/2}I$ and $E_1 = \sqrt{\gamma/2}Z$ for phase damping. Coherence times $T_1$ and $T_2$ were varied from 10 to 100 microseconds.

Measurement errors were modelled as bit-flip processes with probability $p_{\text{meas}}$ varied between 1% and 10%. This analysis showed higher sensitivity to measurement errors than to gate errors, in line with current understanding of quantum-device limitations.

## 3.8 Computational resources and scalability

All simulations were executed on high-performance computing clusters equipped with Intel Xeon Gold 6248 processors operating at 2.5 GHz (20 cores) and 384 GB DDR4 memory. Quantum-circuit simulations employed optimised statevector methods with automatic parallelisation across available cores.

Computational-complexity analysis indicated exponential scaling with qubit number owing to statevector requirements. For $n$-qubit circuits, memory usage scales as $O(2^n)$ and computation time as $O(2^n \cdot \text{circuit depth})$. This constraint limited practical simulations to a maximum of 12 qubits, although near-term quantum hardware may handle larger systems more efficiently.

Wall-clock times for complete hyperparameter optimisation ranged from 2–6 hours per stock for smaller configurations (4–6 qubits) to 12–24 hours for larger systems (8–10 qubits). Classical baseline training typically completed within 30 minutes per stock, underscoring the computational overhead associated with current quantum simulations.

Scalability projections suggest that physical quantum-hardware implementations could markedly reduce these computational demands, as quantum devices inherently manage exponential state spaces without explicit simulation overhead.

## 3.9 Conditional quantum circuits implementation

Regime classification within the conditional quantum-reservoir framework was performed using market-volatility and momentum indicators, with a threshold-based classification scheme defined as follows:

$$\text{Regime} = \begin{cases} \text{Low volatility} & \text{if } \sigma_{20} < 33\text{rd percentile} \\ \text{Medium volatility} & \text{if } 33\text{rd} \leq \sigma_{20} < 67\text{th percentile} \\ \text{High volatility} & \text{if } \sigma_{20} \geq 67\text{th percentile} \end{cases} \tag{20}$$

where $\sigma_{20}$ represents the 20-day rolling volatility of returns.

Each regime employed distinct quantum-circuit architectures optimised for the corresponding market conditions. Low-volatility regimes used sparse entanglement patterns with nearest-neighbour connectivity; medium-volatility regimes employed intermediate connectivity (50% of possible links); and high-volatility regimes used dense, all-to-all entanglement structures.

The regime-specific quantum circuits were pre-trained on historical data segmented by volatility regime, ensuring that each circuit specialised in processing data from its respective market condition. During inference, the regime classifier selected the appropriate quantum circuit based on current market characteristics.

## Data availability

Historical stock price and volume data used in this study are publicly available from the Yahoo Finance (https://finance.yahoo.com ), Alpha Vantage (https://www.alphavantage.co ), and Quandl (https://www.quandl.com ) APIs. Processed datasets containing computed technical indicators and normalised features are available from the corresponding author upon reasonable request, subject to data-use agreements.

Raw performance results—including accuracy, ROC–AUC, precision, and recall metrics for all 30 stocks across all tested configurations—are provided as supplementary data files. Statistical-analysis outputs, including t-test results and confidence intervals, are likewise available.

## Code availability

Complete implementation code for eQCRN, including quantum circuit definitions, training procedures, and evaluation metrics, is available at https://github.com/Panperception/UG_2025_QR. The repository includes PennyLane-based quantum circuit implementations, TensorFlow classical readout layers, and comprehensive evaluation scripts.

Baseline model implementations using scikit-learn and TensorFlow, along with data preprocessing and statistical analysis code, are included in the same repository. Installation instructions, dependency management, and usage examples are provided in detailed documentation.

Noise modelling code for assessing quantum hardware robustness, including implementations of various noise channels and error models, is available as a separate module within the repository.

## Author contributions

A.P. conceived the eQCRN architecture, designed and implemented quantum circuits, performed experiments across target stocks, and conducted statistical analyses, data collection, preprocessing, feature engineering, hyperparameter optimisation, noise modelling, and computational implementation. A.P. also wrote the initial manuscript draft.

W.G. contributed to experimental design and modelling, implemented data processing, performed code review, prepared figures and tables, assisted with data interpretation, and substantially revised the manuscript.

R.J. supervised the research project, provided theoretical guidance on quantum-reservoir computing, assisted with result interpretation, and proofread the manuscript.

All authors contributed equally to result interpretation, manuscript revision, and responses to reviewer comments. They participated in regular research meetings, collaborative analyses, and approved the final version of the manuscript.

## Acknowledgements

The authors thank the LIRA Centre at Lancaster University for providing computational resources and research infrastructure. They gratefully acknowledge valuable discussions with colleagues in quantum computing and financial modelling that helped shape this research, and they thank the wider quantum computing community for developing the open-source tools (PennyLane, Qiskit, and Cirq) that made this work possible.

The authors also thank the anonymous reviewers for their constructive feedback, which substantially improved the manuscript, and acknowledge the broader quantum machine-learning community for establishing the theoretical foundations that enabled this study.

## Funding Declaration

This research was supported by the UK Engineering and Physical Sciences Research Council (EPSRC) under Grant EP/P009727/2 and by the Leverhulme Trust under Grant RF–2019–492. Additional computational resources were provided by the UK National High-Performance Computing facility through allocated time grants.

## Competing interests

The authors declare no competing financial interests related to this work. Neither author has financial relationships with quantum computing companies, financial trading firms, or investment management organizations that could bias the research outcomes. No patents have been filed related to the methods described in this work.

The research was conducted purely for academic purposes without commercial considerations. All software tools used were open-source or freely available academic licenses. No proprietary quantum computing platforms or commercial financial data services were used in ways that would create conflicts of interest.

## References

[1] Bouchaud, J.-P. & Potters, M. *Theory of Financial Risk and Derivative Pricing* 2nd edn (Cambridge University Press, 2018).

[2] Cont, R. Empirical properties of asset returns: stylized facts and statistical issues. *Quant. Finance* **1**, 223–236 (2001).

[3] Harvey, C. R., Liu, Y. & Zhu, H. ... and the cross-section of expected returns. *Rev. Financ. Stud.* **29**, 5–68 (2017).

[4] Campbell, J. Y., Lo, A. W. & MacKinlay, A. C. *The Econometrics of Financial Markets* 2nd edn (Princeton University Press, 2017).

[5] Engle, R. F. GARCH 101: The use of ARCH/GARCH models in applied econometrics. *J. Econ. Perspect.* **15**, 157–168 (2001).

[6] Gu, S., Kelly, B. & Xiu, D. Empirical asset pricing via machine learning. *Rev. Financ. Stud.* **33**, 2223–2273 (2020).

[7] Chen, L., Pelger, M. & Zhu, J. Deep learning in asset pricing. *Management Science* **67**, 4032–4053 (2021).

[8] Fischer, T. & Krauss, C. Deep learning with long short-term memory networks for financial market predictions. *European J. Operational Research* **270**, 654–669 (2018).

[9] Nielsen, M. A. & Chuang, I. L. *Quantum Computation and Quantum Information* (Cambridge University Press, 2010).

[10] Preskill, J. Quantum computing in the NISQ era and beyond. *Quantum* **2**, 79 (2018).

[11] Biamonte, J. et al. Quantum machine learning. *Nature* **549**, 195–202 (2017).

[12] Schuld, M., Sinayskiy, I. & Petruccione, F. An introduction to quantum machine learning. *Contemp. Phys.* **56**, 172–185 (2015).

[13] Wittek, P. *Quantum Machine Learning: What Quantum Computing Means to Data Mining* (Academic Press, 2014).

[14] Havlíček, V. et al. Supervised learning with quantum-enhanced feature spaces. *Nature* **567**, 209–212 (2019).

[15] Chen, J., Wu, Y., Yang, Z. et al. Quantum ensemble learning with a programmable superconducting processor.*npj Quantum Information* **11**, 83 (2025).

[16] Fowler, A. G., Mariantoni, M., Martinis, J. M. & Cleland, A. N. Surface codes: Towards practical large-scale quantum computation. *Phys. Rev. A* **86**, 032324 (2012).

[17] Fujii, K. & Nakajima, K. Harnessing disordered-ensemble quantum dynamics for machine learning. *Phys. Rev. Applied* **8**, 024030 (2017).

[18] Nakajima, K., Fujii, K., Negoro, M., Mitarai, K. & Kitagawa, M. Boosting computational power through spatial multiplexing in quantum reservoir computing. *Phys. Rev. Applied* **11**, 034021 (2019).

[19] Youssef K., Hadi Z., Terrence S., Khabat H. & Christoph S. Frequency- and dissipation-dependent entanglement advantage in spin-network Quantum Reservoir Computing. *arXiv preprint* **2403**.08998 (2024)

[20] Lukoševičius, M. & Jaeger, H. Reservoir computing approaches to recurrent neural network training. *Comput. Sci. Rev.* **3**, 127–149 (2012).

[21] Jaeger, H. The "echo state" approach to analysing and training recurrent neural networks. *German National Research Center for Information Technology GMD Technical Report* **148**, 34 (2001).

[22] Verstraeten, D., Schrauwen, B., D'Haene, M. & Stroobandt, D. An experimental unification of reservoir computing methods. *Neural Networks* **20**, 391–403 (2007).

[23] Schuld, M. & Killoran, N. Quantum machine learning in feature Hilbert spaces. *Phys. Rev. Lett.* **122**, 040504 (2019).

[24] Ghosh, S. et al. Quantum reservoir processing. *npj Quantum Information* **5**, 35 (2019).

[25] Chen, J., Zen, R., Weng, J., Chen, H. & Li, O. Quantum advantage in learning from experiments. *Science* **373**, 1474–1478 (2021).

[26] Arute, F. et al. Quantum supremacy using a programmable superconducting processor. *Nature* **574**, 505–510 (2019).

[27] Jurcevic, P. et al. Demonstration of quantum volume 64 on a superconducting quantum computing system. *Quantum Sci. Technol.* **6**, 025020 (2021).

[28] McClean, J. R., Boixo, S., Smelyanskiy, V. N., Babbush, R. & Neven, H. Barren plateaus in quantum neural network training landscapes. *Nature Commun.* **9**, 4812 (2018).

[29] Ollivier, H. & Zurek, W. H. Quantum discord: a measure of the quantumness of correlations. *Phys. Rev. Lett.* **88**, 017901 (2001).

[30] Bergholm, V. et al. PennyLane: Automatic differentiation of hybrid quantum-classical computations. *arXiv preprint arXiv:1811.04968* (2018).